Resolving CuO chain and CuO_2 plane contributions to the $YBa_2Cu_3O_{7-\delta}$ valence band by standing-wave excited hard x-ray photoelectron spectroscopy

S. Thiess,[1,*] T.-L. Lee,[1,†] C. Aruta,[2] C. T. Lin,[3] F. Venturini,[1,†] N. B. Brookes,[1] B. C. C. Cowie,[1,‡] and J. Zegenhagen[1,§]

[1]*European Synchrotron Radiation Facility (ESRF), 71 Avenue des Martyrs, 38043 Grenoble, France*

[2]*CNR-SPIN, Via del Politecnico 1, 00133 Roma, Italy*

[3]*Max-Planck-Institut für Festkörperforschung, Heisenbergstrasse 1, 70569 Stuttgart, Germany*

(Received 23 October 2014; revised manuscript received 14 May 2015; published 10 August 2015)

We analyzed the valence band (VB) of the 90 K high-temperature superconductor $YBa_2Cu_3O_{7-\delta}$ by photoelectron spectroscopy under standing-wave excitation employing hard x rays. Precisely positioning the standing-wave intensity in the unit cell allows selectively probing the VB yield from the CuO chains and CuO_2 planes, respectively. Both contribute strongly over the whole VB but the spectral weight of the planes is significantly higher than the chains within about 2 eV from the Fermi level. In the x-ray regime, the major contribution to the VB emission is coming from Cu 3*d*.

DOI: 10.1103/PhysRevB.92.075117 PACS number(s): 74.25.Jb, 74.72.Gh, 78.70.Dm, 79.60.−i

I. INTRODUCTION

The electronic structure of the CuO chains and CuO_2 planes largely determines the electronic properties of the 90 K superconductor $YBa_2Cu_3O_{7-\delta}$ (YBCO) [1] (cf. Fig. 1). Hole doping, described by the widely accepted Zhang-Rice scenario [2], is commonly considered introducing superconductivity in the CuO_2 planes. In the present communication we use hard x-ray photoelectron spectroscopy (HAXPES) [3] with standing-wave excitation to unravel the contributions of the CuO chains and CuO_2 planes to the valence band (VB) of YBCO. By placing the maximum of the x-ray wave-field intensity at the chain or plane position, the VB emission from the corresponding site is enhanced, ultimately allowing the decomposition of the VB in the contributions from CuO and CuO_2.

With the help of the x-ray standing wave (XSW) technique [4–6] chemical and electronic information can be retrieved with structural resolution. It has been demonstrated that using the XSW method, the contribution to the VB from individual crystallographic sites can be resolved [7–10]. This helps to understand the relationship between geometric and electronic structure, which is crucial for complex materials of current interest. The large probing depth of HAXPES renders the photoelectron signal truly bulk sensitive, which is particularly important for materials with large unit cells such as YBCO.

The XSW, i.e., a planar interference field, is formed by the incoming and outgoing x-ray beams during Bragg reflection. The x-ray intensity in the unit cell of the reflecting crystal is thus modulated. According to the dynamical theory of x-ray diffraction [11] (DTXD), the position of the XSW in the unit cell can be manipulated. Minima and maxima of the wave-field intensity shift when passing through the Bragg reflection condition by scanning either the incident angle or the energy and eventually exchange their position. Concomitantly monitoring the photoelectron emission of particular chemical species reveals their position within the unit cell of the crystal [12]. High spatial resolution is obtained because the dipole approximation [13] of the electron-photon interaction is largely valid even for hard x rays and the photoelectron is emitted from the core site of the atoms. The dipole approximation holds pretty well even for VB electrons. This was shown convincingly by the experiment of Woicik *et al.* when investigating the XSW-excited VB emission from Cu as well as from Ge and binary semiconductors [7]. The XSW-excited VB emission allows us here to assign particular density of states (DOS) of the YBCO VB to the CuO chains and CuO_2 planes. They are occupied by two species of the same element, i.e., Cu(1) and Cu(2) (cf. Fig. 1), residing at symmetry-inequivalent lattice sites.

II. YBCO STRUCTURE, ELECTRONIC STRUCTURE AND X-RAY CROSS SECTIONS

The thirteen atoms in the orthorhombic unit cell of YBCO occupy eight by symmetry nonequivalent lattice sites, i.e., one barium, one yttrium, two copper, and four oxygen sites, as indicated in the sketch of the unit cell shown in Fig. 1(a). The partial DOS (pDOS) of YBCO for the different lattice sites has been calculated by different technical approaches [14–18]. All studies agree in the finding that the YBCO VB is composed to ≈95% of Cu 3*d* and oxygen 2*p* states, with the strongest contribution coming from the Cu states. Yttrium and barium contribute only very little to the VB DOS. According to the calculations, the pDOS of Cu(1) and Cu(2) are different [14–18] with the pDOS of Cu(1) dominating at higher binding energy (BE) $\gtrapprox$3 eV, with the notable exception of some additional weight close to the Fermi level, and the pDOS of Cu(2) dominating at lower BE [cf. Fig. 1(b)].

*Present address: DESY, Notkestrasse 85, 22607 Hamburg, Germany.

†Present address: Diamond Light Source Ltd., Harwell Science and Innovation Campus, Didcot OX11 0DE, UK.

‡Present address: Australian Synchrotron Company Ltd., 800 Blackburn Road, Clayton, VIC 3168, Australia.

§Present address: Diamond Light Source Ltd., Harwell Science and Innovation Campus, Didcot OX11 0DE, UK; jorg.zegenhagen@diamond.ac.uk

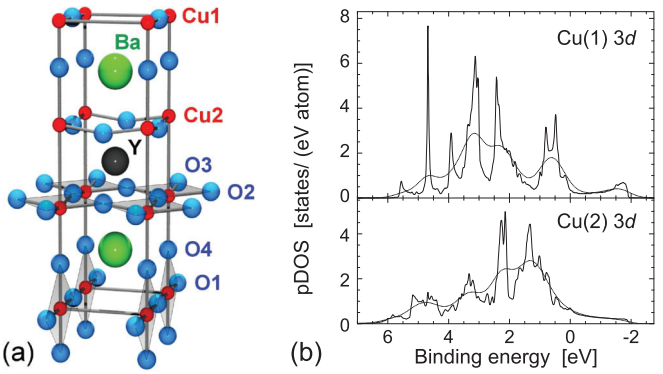

FIG. 1. (Color online) (a) Structure of $YBa_2Cu_3O_7$, space group $Pmmm$, lattice parameter $c = 1.168$ nm. The fourfold oxygen coordination of the chain Cu(1) sites and the in-plane Cu(2) sites is shown shaded. (b) Calculated pDOS at the Cu(1) and Cu(2) sites adapted from Larbaoui *et al.* [17]. Dotted lines: pDOS broadened by 0.75 eV to account for the experimental resolution.

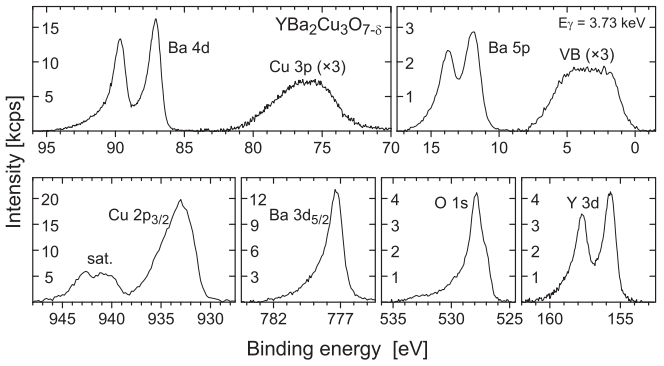

FIG. 2. Photoelectron core level spectra from a low-temperature cleaved $YBa_2Cu_3O_{7-\delta}$ single crystal with 3.73 keV excitation energy.

The photoelectron intensity from the VB is proportional to the local density of states (lDOS) and the photoelectric cross section. The latter depends on element and electronic state, specifically on the shape of the electron wave function close to the core. The cross section is strongly energy dependent, which offers a means to selectively enhance or suppress features of specific elements and states in the VB yield. Here, the excitation by hard x rays highlights the contribution of Cu 3d states to the VB yield since the Cu 3d cross section is more than a factor of ten larger than the O 2p cross section [19].

III. EXPERIMENTAL

The XSW HAXPES experiments were performed in the UHV chamber of the undulator beamline ID32 [20] at the European Synchrotron Radiation Facility (ESRF) in Grenoble, France. The photoelectron analyzer was mounted in the horizontal polarization plane of the beam at an angle of 45° with respect to the polarization direction. The Si(111) monochromator provided an energy resolution of $\Delta E_\gamma \approx 1.4\times10^{-4} \times E_\gamma$ at the used x-ray energies E_γ, which dominated the overall instrumental resolution. The used $YBa_2Cu_3O_{7-\delta}$ twinned single crystals with $\delta = 0.05$ and typically 0.5 mm × 10 mm^2 (thickness × area) had been grown by the traveling solvent float zone technique [21]. When mounted strain-free to avoid lattice distortions they were found earlier to be suitable for XSW measurements [22]. However, in order to minimize the broadening of the YBCO rocking curves, due to the mosaic spread of the crystals, the XSW measurements were carried out at near-normal incidence by scanning the energy of the monochromator. The samples were cleaved in the *ab* plane by blade in UHV. They were cooled and kept at a temperature of <40 K during cleaving and subsequent measurements [23]. The background pressure was better than 10^{-10} mbar. Of the (001) surface exposed by cleaving, a region of a few hundredths of mm^2 was used for the XSW/HAXPES measurements.

IV. EXPERIMENTAL RESULTS: CORE LEVEL ANALYSIS

In Fig. 2 typical photoelectron spectra from a cleaved crystal are shown. The O 1s spectrum exhibits a characteristic shoulder towards low BE and a tail on the high-BE side, as has been reported previously for a clean surface [24]. YBCO cleaves predominantly in the $BaCuO_3$ plane [25] and the asymmetry of the Ba $3d_{5/2}$ line was assigned earlier to BaO surface termination of the cleaved crystal [26].

For the XSW measurements we utilized YBCO(00ℓ) Bragg reflections with $\ell = 5$, 6, 7 at around 2.661 keV, 3.193 keV, and 3.725 keV, respectively [23]. Traversing the (00ℓ) Bragg reflections, the wave-field planes, which are parallel to the *ab* planes of YBCO with a spacing c/ℓ, move along the c axis of the YBCO crystal. The x-ray photoelectron spectra were recorded for a discrete set of excitation energies within the range of reflection, i.e., for different positions of the XSW within the YBCO unit cell.

In Fig. 3 the (005), (006), and (007) XSW results for the integrated YBCO VB and core level yields are shown and the visible strong modulations testify to the high spatial resolution. It is well known that the satellite signal of the Cu $2p_{3/2}$ peak shown in Fig. 2 originates from Cu in the intrinsic bulk material exclusively, while the main peak can also contain contributions from reduced Cu typically present in nonintrinsic phases [27]. Thus, the XSW yield of the Cu $2p_{3/2}$ main peak and its satellite have been analyzed separately (cf. Fig. 3). Quantitative results of the fits to the data [28] in Fig. 3 corroborated the visual impression that the XSW yield for the main peak and the satellite structure are indistinguishable. This provides further proof of the absence of extrinsic phases which could influence the VB yield [23].

According to the YBCO crystal structure, the XSW modulation of the Y $2p_{3/2}$ emission is expected to be in counterphase with the emission from the three other elements for the (005) reflection. This is markedly reflected by the measurement, since only the Y $2p_{3/2}$ curve is peaked clearly on the left of the marker line in Fig. 3. For the (006) reflection all XSW modulations are expected to be in phase, in agreement with the experimental result, with the maxima of all curves clearly on the right-hand side of the marker line. For the (007) reflection the Y, Ba, and Cu curves are all peaked slightly to the right of the marker line, whereas the oxygen curve is peaked slightly

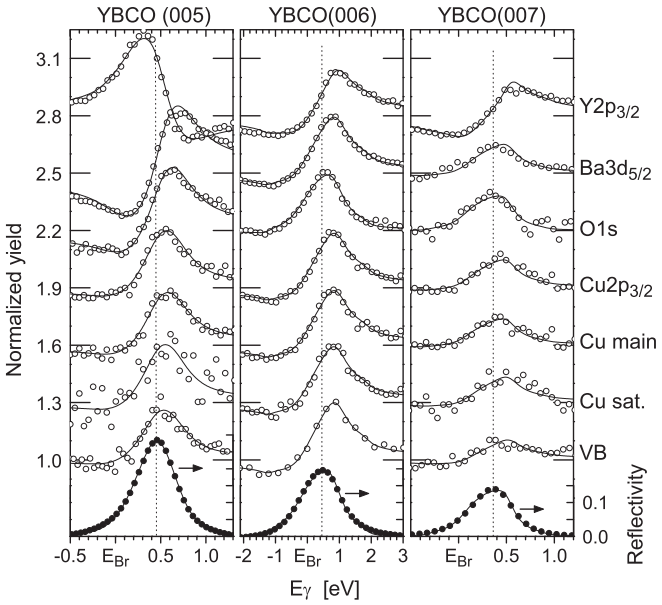

FIG. 3. Core and valence level XSW yield for YBCO(00ℓ) reflections at energies E_γ around Bragg energies E_{Br} of 2.661, 3.193, and 3.725 keV for $\ell = 5$, 6, and 7, respectively. Corresponding rocking curves are shown on the bottom of the plots. Symbols represent the Shirley background subtracted peak integral of the corresponding electronic levels recorded in constant initial state mode at the specific E_γ and lines are fits to the data based on the DTXD [11] according to standard XSW procedure [6,28]. The movement of the wave field (spacing of c/ℓ) through the YBCO unit cell along the c axis causes strong modulation of the electron yields. The curves for the individual electronic levels, as labeled on the right-hand side, are offset for clarity. Error bars are about the size of the symbols or smaller.

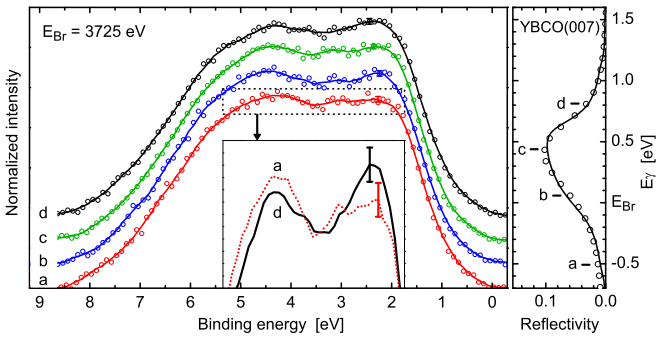

FIG. 4. (Color online) XSW results employing the YBCO(007) reflection. VB yield curves (left diagram) recorded at four different positions on the YBCO(007) rocking curve (right-hand diagram). Wave-field maxima are on the Cu(1) and Cu(2) site at a and d, respectively. VB spectra: Symbols are data and lines are guides to the eye; the curves are normalized and offset on the vertical scale for clarity. The inset shows the indicated top part of curve a (dashed) and d (solid line) without offset on an enlarged scale with the size of the error bars indicated. YBCO(007) rocking curve: Symbols are data and line is fit to the data with the help of DTXD.

to the left, since the signal from oxygen is indeed expected to be in counterphase [23].

For the (005) and (006) reflections, Cu(1) and Cu(2) are excited in phase and the Cu yield is strongly modulated. For the YBCO(007) reflection the XSW maxima pass first the Cu(1) and then the Cu(2) site when traversing the reflection range by increasing the energy and Cu(1) and Cu(2) are consequently excited in counterphase. Correspondingly, the core level Cu signal originating from both Cu species is only weakly modulated.

V. EXPERIMENTAL RESULTS: VALENCE BAND ANALYSIS

Evidently, for all three reflections, the integrated emission from the VB follows very closely the core level signal from copper (and not oxygen), which was confirmed quantitatively by the numerical results of the fit [23,28]. This proves that the YBCO VB yield is dominated by the emission from the Cu sites, as expected from the major contribution of Cu to the DOS [14–18] and the fact that the cross section for Cu is much larger than for oxygen in the x-ray regime.

The information about the site-specific contributions to the valence yield is contained in the variation of the VB line shape within the range of Bragg reflection. For the YBCO(007) reflection VB spectra were recorded at four different photon energies within the range of the (007) Bragg reflection. The x-ray energy, i.e., the monochromator, was found to be reliable within ± 0.1 eV over the course of the measurement, which took about two hours. Taking this possible error into account, the instrumental resolution was better than 0.75 eV. Three different measurements on two samples were carried out, yielding equivalent results. The result of one measurement is shown in Fig. 4. Because of variations of the intensity of the beam on the sample, causing changes in the emitted photoelectron intensity, the VB spectra are normalized. The main shape of the VB, featuring two broad humps at around 2.5 eV and 4.5 eV binding energy, agrees well with published data [29–32]. The yield at the Fermi edge is rather low, less than 5% of the VB maximum [33].

The information about the precise position of the wave-field maxima in the YBCO unit cell is encoded in the recorded rocking curve signal. It can be retrieved by fitting a function calculated with the help of the DTXD to the recorded YBCO(007) reflectivity data [6,11]. The wave-field intensity maxima in the unit cell move from Cu(1) to Cu(2) (Fig. 1) when scanning from lower to higher energy (cf. Fig. 4). The variations in the shape of the VB emission in response to the movement of the interference field are weak but clearly distinguishable. With the maxima at Cu(2) there is larger spectral weight close to the Fermi level whereas with the maxima at Cu(1) there is a slight increase in intensity at higher BE, as the inset in Fig. 4 shows more clearly.

VI. XSW DECOMPOSITION OF THE VALENCE BAND YIELD

With the help of the site-specific XSW excitation, the recorded spectra can be decomposed into local yields from the CuO chains and the CuO_2 planes by a straightforward procedure. We assume that the VB photoelectron yield is dominated by emission from Cu. Thus, the VB yield from

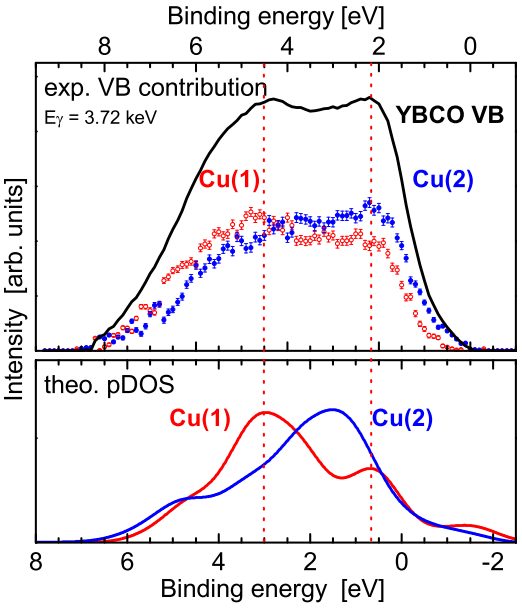

FIG. 5. (Color online) XSW analysis of the contributions of Cu(1) (chains) and Cu(2) (planes) to the YBCO VB emission determined from the XSW data recorded for the YBCO(007) reflection shown in Fig. 4 (upper diagram) compared with the calculated pDOS from Fig. 1(b) (lower diagram) broadened by 1.2 eV, which is 50% larger than the instrumental resolution of 0.75 eV. In a heuristic approach, both diagrams are shifted relative to each other to better align the weight of the spectra.

electrons with BE E_B excited by the (007) XSW can be to very good approximation written as [7]

$$Y(E_B) \sim p_1(E_B)\cdot\sigma_1[1+R+2\sqrt{R}\cos(v+\mathbf{h}\cdot\mathbf{r}_1)] + p_2(E_B)\cdot\sigma_2[1+R+2\sqrt{R}\cos(v+\mathbf{h}\cdot\mathbf{r}_2)]. \quad (1)$$

In this equation, $p_{1,2}(E_B)$ is the site-specific DOS, or local DOS of the valence electrons with E_B at the position of the Cu(1) and Cu(2) atoms $\mathbf{r}_1$ and $\mathbf{r}_2$, respectively, R is the YBCO(007) reflectivity, v is the phase of the XSW, which changes by π rad when passing the Bragg reflection, and $\mathbf{h}$ is the (007) diffraction vector. We assume that the photo cross section $\sigma_{1,2} = f(E_B, E_\gamma)$ for both copper atoms is constant over the ≈8 eV range of binding energies. Consequently, measuring $Y(E_B)$ for two values of v suffices for determining $p_{1,2}\sigma_{1,2}$ as a function of E_B by numerically solving the two equations. Furthermore, it is legitimate to assume that $\sigma_1 = \sigma_2$. The (normalized) site-specific density of states of Cu(1) and Cu(2) obtained in this way from the data shown in Fig. 4 using four values of v for a best fit is shown in Fig. 5.

VII. DISCUSSION OF RESULTS

Because the VB spectra were normalized for the analysis, only the shape and not the total intensity of the lDOS can be interpreted. The VB lDOS shown in Fig. 5 becomes similar to the calculated pDOS shown in Fig. 1, when the latter is broadened beyond the experimental resolution, by 1.2 eV as shown in the lower panel of Fig. 5. With two characteristic maxima, in particular the shape of the pDOS of Cu(1) is reasonably well reproduced, but the experimental lDOS shows less structure. For both Cu species the experimental lDOS is much broader with an almost flat top in the range of about 2 to 5 eV binding energy. The experimental lDOS cannot be brought into agreement with the theoretical prediction. The two characteristic maxima for Cu(1) and Cu(2) are almost 1 eV further apart, since the lDOS of Cu(2) is shifted to lower binding energy, i.e., closer to the Fermi edge with respect to Cu(1).

We can think of several reasons for the broader features in the experimental lDOS such as (1) experimental deficiencies, (2) broadening due to photoelectron recoil, or (3) final state effects. We believe that we can largely exclude experimental issues. The width of the lDOS (and the VB) exceeds the experimental resolution by far and three different measurements on two samples gave the same results. Furthermore, our overall VB shape with relatively sharp upward and downward slopes agrees well with the findings of earlier experimental studies [29,30,32]. Photoelectron recoil can account for a broadening ΔE ($\approx E_\gamma \times m_e/M_{Cu}$), which is about 30 meV and thus practically insignificant. Previous XSW investigations of the VB yield of correlated transition metal oxides had also shown significantly broadened features compared to the calculated pDOS, reflected by a pronounced tail of the experimental "lDOS" to higher binding energy. This was properly explained by final state effects and good agreement with theory was achieved by convoluting the calculated pDOS with a Doniach-Šunjić line shape [8]. Such final state effects cannot fully explain the deviation of Cu(1) and Cu(2) partial yields from the theoretical pDOS. The experimental spectra are broad but with and almost trapezoidal shape, relatively steep flanks, without significant tail to higher binding energy. Other, yet not considered factors in the electron emission process may be responsible for the observed shape of the partial yields. However, we are tempted to suspect that also the theoretical description of the ground state electronic structure of YBCO may need to be revisited. This is additionally strongly suggested by the fact that the experimental lDOS of Cu(2) exceeds the lDOS of Cu(1) considerably at lower binding energy, which is not predicted by the calculations.

VIII. VALENCE BAND INVESTIGATION WITH SOFT X-RAYS

Before summarizing we should mention that we also performed XSW PES measurements using the (001) reflection with soft x-rays (0.564 keV) at a Bragg angle of 70°. The results turned out not to be reliable since the VB shape was found to be not reproducible to the accuracy needed (see Supplemental Material [23]), which was required to be higher than for the (007) reflection because of an about five times lower reflectivity and thus much smaller changes in the VB shape introduced by the XSW movement. Owing to the small electron escape depth (≈1 nm), minor changes in the electron escape angle and/or of the position of the beam on the sample caused changes of the VB shape, overshadowing those induced by the

XSW movement. It is known that the vacuum-cleaved surface is not homogeneous, owing to different terminations [34], and Ba 5*p* surface components can be observed [26,32]. Furthermore, the electronic structure of the near-surface region of the cleaved YBCO will be affected simply by the truncation of the crystal. Because of the large *c*-axis lengths of the YBCO of 1.2 nm, a larger electron escape depth (around 4 nm at 3.7 keV) appears to be mandatory for avoiding any influence of the surface on the electron yield recorded from YBCO crystals.

IX. CONCLUSIONS

In conclusion, we used the XSW technique in combination with HAXPES to analyze the VB structure of YBCO. By positioning the YBCO(007) interference field properly, we can selectively identify the emission from two different lattice sites of the same element, here Cu. Thus the VB XSW technique is complementary to resonant VB photoelectron spectroscopy, which is element specific, but would not be able to distinguish between the two Cu species in this case. As expected, the YBCO VB emission is dominated by Cu 3*d* states in the x-ray regime, but unexpectedly both Cu species contribute strongly over the whole width of the VB and the plane Cu(2) contributes closer to the Fermi level more spectral weight than predicted by existing calculations. A minor contribution from oxygen to the yield would not change the overall interpretation since O(1) and O(4) are strongly hybridized with Cu(1) and are for the (007) reflection in phase with Cu(1) whereas O(2) and O(3) are hybridized and emit in phase with Cu(2) [14–18]. Thus, close (≈1 eV) to the Fermi level the electronic states of YBCO appear to be localized, in agreement with the conclusions of an ARPES study performed on CuO-chain and CuO_2-plane terminated terraces of $YBa_2Cu_3O_8$ [34]. XSW measurements using the YBCO(001) reflection at around 565 eV were not successful which demonstrates that, even when the surface is clean, care is needed when interpreting the VB spectra of materials with such a large unit cell. Finally we would like to mention that with significantly better instrumental resolution (<100 meV) it should be possible to test the origin of the electronic states and quasiparticles right at the Fermi level which are responsible for transport and superconductivity.

ACKNOWLEDGMENTS

We would like to thank Helena Isern and Lionel André for skillful technical assistance at the ID32 beamline. The German Bundesministeriums für Bildung und Forschung is acknowledged for financial support under Contract No. 05KS4GU3/1.

[1] M. K. Wu, J. R. Ashburn, C. J. Torng, P. H. Hor, R. L. Meng, L. Gao, Z. J. Huang, Y. Q. Wang, and C. W. Chu, Phys. Rev. Lett. **58**, 908 (1987).
[2] F. C. Zhang and T. M. Rice, Phys. Rev. B. **37**, 3759 (1988).
[3] See e.g., *Proceedings of the Workshop on Hard X-ray Photoelectron Spectroscopy*, edited by Jörg Zegenhagen and Christof Kunz Nucl. Instrum. Methods Phys. Res., Sect. A Vol. 547 (Elsevier, Amsterdam, 2005), p. 1.
[4] B. W. Batterman, Phys. Rev. Lett. **22**, 703 (1969).
[5] J. Zegenhagen, Surf. Sci. Rep. **18**, 199 (1993).
[6] For a comprehensive description, see *The X-Ray Standing Waves Technique: Principles and Applications*, edited by Jörg Zegenhagen and Alexander Y. Kazimirov (World Scientific, Singapore, 2013).
[7] J. C. Woicik, E. J. Nelson, D. Heskett, J. Warner, L. E. Berman, B. A. Karlin, I. A. Vartanyants, M. Z. Hasan, T. Kendelewicz, Z. X. Shen, and P. Pianetta, Phys. Rev. B **64**, 125115 (2001).
[8] J. C. Woicik, M. Yekutiel, E. J. Nelson, N. Jacobson, P. Pfalzer, M. Klemm, S. Horn, and L. Kronik, Phys. Rev. B **76**, 165101 (2007).
[9] S. Thiess, T.-L. Lee, F. Bottin, and J. Zegenhagen, Solid State Commun. **150**, 553 (2010).
[10] J. C. Woicik, in *The X-ray Standing Wave Technique, Principles and Applications*, edited by Jörg Zegenhagen and Alexander Kazimirov (World Scientific, Singapore, 2013), Chap. 12 and Chap. 26.
[11] M. v. Laue, *Röntgenstrahl-Interferenzen* Akademische Verlagsgesellschaft, Becker & ErlerKolm.-Ges., Leipzig, 1941 (Akademische Verlagsgesellschaft, Frankfurt, 1960); B. Batterman and H. Cole, Rev. Mod. Phys. **36**, 681 (1964).
[12] B. W. Batterman, Phys. Rev. **133**, A759 (1964).
[13] In the dipole approximation, the exponential $e^{2\pi i\mathbf{kr}}$ of the *E*-field operator in the matrix element, describing the photoelectric process, is simply replaced by 1, the first term of its corresponding representation in a Taylor series $[1 + 2\pi i\mathbf{kr} - \pi^2(\mathbf{kr})^2 - ...]$.
[14] S. Massida, Jaejun Yu, A. J. Freeman, and D. D. Koelling, Phys. Lett. **122**, 198 (1987).
[15] H. Krakauer, W. E. Pickett, and R. E. Cohen, J. Supercond. **1**, 111 (1988).
[16] H. Kim and J. Ihm, Phys. Rev. B **51**, 3886 (1995).
[17] K. Larbaoui, A. Tadjer, B. Abbar, H. Aourag, B. Khelifa, and C. Mathieu, J. Alloys Compd. **403**, 1 (2005).
[18] Maciej Łuszczek, Physica C **469**, 1892 (2009).
[19] M. B. Trzhaskovskaya, V. I. Nefedov, and V. G. Yarzhemsky, At. Data Nucl. Data Tables **77**, 97 (2001).
[20] J. Zegenhagen, B. Detlefs, T.-L. Lee, S. Thiess, H. Isern, L. Petit, L. André, J. Roy, Y. Mi, and I. Joumard, J. Electron Spectrosc. Relat. Phenom. **178**, 258 (2010).
[21] C. T. Lin, W. Zhou, W. Y. Liang, E. Schönherr, and H. Bender, Physica C **195**, 291 (1992).
[22] S. Thiess, T.-L. Lee, C. T. Lin, L. X. Cao, C. Aruta, S. Warren, B. C. C. Cowie, and J. Zegenhagen, Phys. Status Solidi B **233**, R5 (2002).
[23] See Supplemental Material at http://link.aps.org/supplemental/10.1103/PhysRevB.92.075117 for more details on sample preparation and characterization, for more details on the choice of the YBCO(00ℓ) reflections, for the expected XSW results in terms of coherent position and coherent fraction for the used YBCO reflections, for the quantitative results of the XSW measurements for the three (00ℓ) reflections, as well as for more details on the attempt of using the (001) reflection at 563.5 eV.

[24] C. R. Brundle and D. E. Fowler, Surf. Sci. Rep. **19**, 143 (1993).

[25] Kalobaran Maiti, Jörg Fink, Sanne de Jong, Mihaela Gorgoi, Chentian Lin, Markus Raichle, Vladimir Hinkov, Michael Lambacher, Andreas Erb, and Mark S. Golden, Phys. Rev. B **80**, 165132 (2009).

[26] R. P. Vasquez, J. Electron Spectrosc. Relat. Phenom. **66**, 241 (1994).

[27] W. R. Flavell and R. G. Egdell, Phys. Rev. B **39**, 231 (1989).

[28] When quantitatively evaluating XSW data, the yield function $Y = I_0[1 + R + 2F\sqrt{R}\cos(v + 2\pi P)]$ is fitted to the data with the normalization constant I_0 and the two parameters coherent fraction F and coherent position P, representing the numerical result of the XSW measurement [6].

[29] P. Steiner, V. Kinsinger, I. Sander, B. Siegwart, S. Hüfner, and C. Politis, Z. Phys. B: Condens. Matter **67**, 19 (1987).

[30] A. J. Arko, R. S. List, R. J. Bartlett, S.-W. Cheong, Z. Fisk, J. D. Thompson, C. G. Olson, A.-B. Yang, R. Liu, C. Gu, B. W. Veal, J. Z. Liu, A. P. Paulikas, K. Vandervoort, H. Claus, J. C. Campuzano, J. E. Schirber, and N. D. Shinn, Phys. Rev. B **40**, 2268 (1989).

[31] B. W. Veal and Chun Gu, J. Electron Spectrosc. Relat. Phenom. **66**, 321 (1994).

[32] Matthias C. Schabel, C.-H. Park, A. Matsuura, Z.-X. Shen, D. A. Bonn, Ruixing Liang, and W. N. Hardy, Phys. Rev. B **57**, 6090 (1998).

[33] This may indicate that the DOS at E_F is dominated by oxygen [14, 15, 16, 17, 18], the emission of which is diminished by the small O $2p$ cross section in the x-ray regime.

[34] T. Kondo, R. Khasanov, J. Karpinski, S. M. Kazakov, N. D. Zhigadlo, T. Ohta, H. M. Fretwell, A. D. Palczewski, J. D. Koll, J. Mesot, E. Rotenberg, H. Keller, and A. Kaminski, Phys. Rev. Lett. **98**, 157002 (2007).